Indian Journal of Chemistry
Vol. 64, November 2025, pp. 1022-1037
DOI: 10.56042/ijc.v64i11.16314

Synthesis, DFT studies, antimicrobial, radical scavenging activity, and QSAR studies of 3-((E)-((pyridin-2-yl)methyl imino)methyl)-4*H*-chromen-4-one

Kandala Satyanarayana[a], Koppu Suneetha[b], Munagala Alivelu[c] & Natte Kavitha*[d]

[a] Department of Chemistry, Government Degree College (Autonomous), Narsampet 506 132, Telangana, India

[b] Department of Chemistry, SRR Government Arts and Science College (Autonomous), Karimnagar 505 001, Telangana, India

[c] Department of Chemistry, Government Degree College, Gajwel 502 278, Telangana, India

[d] Department of Chemistry, Government Degree College, Bhupalpally 506 169, Telangana, India

E-mail: nattekavitha2008@gmail.com, satyanarayana.kandala@gmail.com, skoppu67@gmail.com, munagalaalivelu@gmail.com

Received 10 January 2025; accepted (revised) 6 October 2025

The 3-((E)-((pyridin-2-yl) methyl imino) methyl)-4*H*-chromen-4-one (PMMC) chromone derivative has been synthesized, characterized by FT-IR, ^{1}H NMR, and mass spectrometry. Molecular properties have been computed using the B3LYP method with B3LYP/6-311++ G (d,p) basis set in the gas phase. The stability and charge delocalization of the molecule have also been deliberated by natural bond orbital (NBO) analysis. The nonlinear optical (NLO) value is 1224.5707×10^{-30} esu, which helps to find the potential of PMMC as a good NLO candidate. Molecular electrostatic potential (MEP) surface and E_{HOMO}-E_{LUMO} energy gap (4.677095 eV) assist the feasibility of charge transfer in the title molecule. The Mullikan's population analysis provides a depiction of charge distribution. Based on the drug likeness principles of PMMC, it exhibits ideal physicochemical and pharmacokinetic properties. The title molecule has been examined for activity against two gram-positive bacteria such as *Staphylococcus aureus* and *Bacillus subtilis* and two gram-negative bacteria such as *Klebsiella pneumoniae* and *Escherichia coli*. It has also been tested for anti-fungal activity and radical scavenging effect.

Keywords: Chromone, NBO, NLO, Druglikeness, Antibacterial activity

Schiff bases have been one of the most significant co-ordination chemistry chelating systems, and utilization of these compounds in materials science has developed rapidly. In 1864, the condensation between a carbonyl compound and an amine leading to the formation of a Schiff base was identified by Hugo Schiff, a German Chemist[1]. Schiff base ligands are easier to generate with aldehydes[2] than with ketones. Numerous physiologically significant Schiff bases have been identified in literature with antibacterial[3], antifungal[4], anticonvulsant[5], and anticancer[6] properties. Since the last few decades, researchers from different fields have paid significant attention to discovering or synthesizing novel derivatives of parent coumarins. Coumarin derivatives have significant biological activity, such as "anti-thrombotic and Vasodilatory"[7], anticancer[8], antifungal[9], antibacterial[10], antioxidant[11], and antitumorigenic[12], Anticoagulant[13], antiplasmodial[14] hypotensive[15], anthelmintic[16], anti-Parkinson Disease medicinal products, inhibition of platelet aggregation[17], anti-neurodegenerative[18], anti-HIV[19], molluscidal[20] and bioanalytical reagents[21]. Not only can coumarins be utilised to cure cancer, they can also be used to relieve radiation side effects[22]. Several structurally distinct natural and synthetic coumarin compounds have also been reported as DNA-Gyrase inhibitors.

Density functional theory (DFT), a cost-effective method for calculating molecular structures, vibration frequencies, and chemical reaction energy, has lately gained widespread acceptance in the quantum chemistry field. Numerous investigations have shown how incredibly accurate DFT calculations of molecule structures and vibration frequencies are. Computational methods have occasionally been used to determine the characteristics of molecules[23,24]. In order to analyse the topologies and energies of electronic ground states in both their static and dynamic forms, DFT is crucial. It can be applied to determine dynamic characteristics and excitation energies.

Because of the high degree of bio-activity shown by coumarin heterocyclic analogs, we have focused on the design of novel structural entities that incorporate both of these structural moieties into a

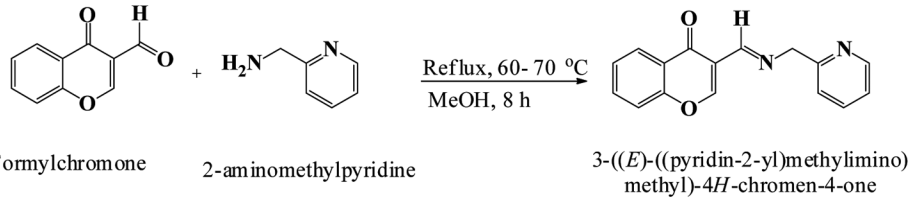

3- Formylchromone 2-aminomethylpyridine 3-((*E*)-((pyridin-2-yl)methylimino) methyl)-4*H*-chromen-4-one

Scheme 1 — Synthesis of 3-((E)-((pyridin-2-yl)methylimino)methyl)-4*H*-chromen-4-one (PMMC)

single molecular scaffold. For these reasons, we chose the PMMC molecule in this study. Infrared (IR), mass, and nuclear magnetic resonance (^{1}H, ^{13}C) techniques were employed for the structural identifications of organic compound under the investigation. The theoretical method of density functional theory (DFT), combining the hybrid exchange-correlation functional Becke-3-Lee-Yang-Parr (B3LYP) with the standard 6-311G++(d,p) basis set, has been providing consistent and accurate calculation of molecular structures for many organic molecules[25]. Theoretical analysis on molecular structure, HOMO-LUMO, NLO, NBO and MEP map of the synthesized compound was carried out by using the Gaussian 09 program with the DFT method. We can determine whether the chosen techniques are reliable for predicting the properties of other structurally comparable molecules by comparing experimental and theoretical results. Drug likeness principles are based on the rules of Lipinski and Veber considering that the header molecule had the ideal physicochemical and pharmacokinetic properties. The title molecule was examined for gram-positive bacteria such as *Staphylococcus aureus* and *Bacillus subtilis* and two gram-negative bacteria such as *Klebsiella pneumoniae* and *Escherichia coli* and it was tested for antifungal activity.

Experimental Section

Synthesis and experimental methods

A solution of 3-formyl chromone (1.1 g, 6 mmol) in 15 mL methanol solvent is condensed with 2-aminomethyl pyridine (0.7 mL, 6.5 mmol) at 65-70°C for 8 h. After the addition of 2-aminomethyl pyridine the reaction mixture turns into a brown colour. The reaction was monitored by TLC, and after it was complete, the mixture was filtered, washed with diethyl ether, and vacuum-dried. Then brown coloured solid was obtained as the final product, which was recrystallized from ethanol to get the pure compound (Scheme 1). The yield is 71.1%, m.p.212°C. IR(KBr): 1645 (C=O),1551 (C=N), 1428 (C=C) 1186 cm^{-1} (C-O); HRMS: *m/z* 265.09[M+H]$^+$. Anal. Calcd for $C_{16}H_{12}N_2O_2$: C, 72.71; H, 4.59; N, 10.61. Found: C, 72.63; H, 4.44; N, 10.32%.

Instrumentation

The FT-IR spectrum of the PMMC compound diluted in the KBr pellets was recorded on a Thermo Electron Nexus 670 spectrophotometer in the range of 400-4000 cm^{-1}. Both the ^{1}H NMR and ^{13}C NMR measurements were carried out using a Bruker AV600 NMR spectrometer with tetramethylsilane (TMS) as an internal standard in dimethyl sulfoxide (DMSO) solvent.

DPPH radical scavenging assay

The antioxidant activity of PMMC was demonstrated by its capacity to neutralize the stable free radical 2, 2-diphenyl-1-picrylhydrazyl (DPPH). The highest electronic absorption band of the stable free radical DPPH is observed at 517 nm, where its color changes from purple to yellow. The absorption band narrows when the DPPH radical's odd electron combines with a hydrogen atom from an antioxidant to form the reduced DPPH-H.

Computational Details

Gaussian09 software was used for the theoretical study of the properties of the title compound. By using the DFT method at the B3LYP/6-311++G(d,p) level, calculations on molecular structure were carried out. The optimized geometries are minima on the corresponding potential energy hypersurfaces. Due to the neglect of the harmonicity effect, certain theoretically computed frequencies are found to be in agreement with that of the experimental frequencies. Therefore, the calculated values are in good agreement with the experimental ones. Natural bonding orbital calculations were calculated using the NBO 3.1 program using the Gaussian 09W package[26]. The compound's hyperpolarizability and NLO application were tested. The molecular electrostatic potential which summarizes the charge distribution of the molecule was examined to find out and

electrophilic regions of the molecule. Gauss view 6.0 visualization program is utilized to view the shape of HOMO and LUMO[27]. Frontier molecular orbitals were analyzed to show the distribution and transition of electrons.

Results and Discussion

Optimized molecular structure

Using a consistent atom numbering method, the optimized structural parameters of PMMC were compiled in Table 1 and displayed in Fig. 1. The

Table 1 — The PMMC optimized geometrical parameters bond length, bond angle with B3LYP/6-311 G++ (d, p) method

Atom	Bond length(Å)	Atom	Bond angle (°)	Atom	Dihydral angle (°)
R(1,2)	1.38	A(2,1,6)	120.5622	D(6,1,2,3)	0.0138
R(1,6)	1.40	A(2,1,7)	119.4975	D(6,1,2,8)	-179.603
R(1,7)	1.07	A(6,1,7)	119.4975	D(7,1,2,3)	179.867
R(2,3)	1.40	A(1,2,3)	118.8924	D(7,1,2,8)	0.220
R(2,8)	1.07	A(1,2,8)	122.096	D(2,1,6,5)	-0.0175
R(3,4)	1.39	A(3,2,8)	119.0117	D(2,1,6,11)	179.9895
R(3,16)	1.32	A(2,3,4)	121.4571	D(7,1,6,5)	179.366
R(4,5)	1.40	A(2,3,16)	117.4832	D(7,1,6,11)	0.0068
R(4,9)	1.44	A(4,3,16)	121.0596	D(1,2,3,4)	0.0096
R(5,6)	1.38	A(3,4,9)	121.2068	D(1,2,3,16)	--179.9354
R(5,10)	1.07	A(5,4,9)	119.9716	D(8,2,3,4)	179.9867
R(6,11)	1.07	A(4,5,6)	120.4264	D(8,2,3,16)	0.0417
R(9,12)	1.42	A(4,5,10)	117.2675	D(2,3,4,5)	-0.0288
R(9,15)	1.25	A(6,5,10)	122.306	D(2,3,4,9)	179.9177
R(12,13)	1.35	A(1,6,5)	119.8403	D(16,3,4,5)	179.9143
R(12,17)	1.46	A(1,6,11)	119.8242	D(16,3,4,9)	-0.1393
R(13,14)	1.08	A(5,6,11)	120.3355	D(2,3,16,13)	-179.9142
R(13,16)	1.37	A(4,9,12)	113.9757	D(4,3,16,13)	0.1406
R(17,18)	1.07	A(4,9,15)	122.7906	D(3,4,5,6)	0.0249
R(17,19)	1.09	A(12,9,15)	123.2337	D(3,4,5,10)	179.9952
R(18,22)	1.47	A(9,12,13)	121.0657	D(9,4,5,6)	-179.9222
R(20,22)	1.09	A(9,12,17)	117.965	D(9,4,5,10)	0.048
R(21,22)	1.10	A(13,12,17)	120.9688	D(3,4,9,12)	-0.0854
R(22,23)	1.54	A(12,13,14)	122.9186	D(3,4,9,15)	179.8808
R(23,24)	1.39	A(12,13,16)	124.3506	D(5,4,9,12)	179.8604
R(23,28)	1.34	A(14,13,16)	112.7308	D(5,4,9,15)	-0.1734
R(24,25)	1.39	A(3,16,13)	118.3406	D(4,5,6,1)	-0.0023
R(24,30)	1.08	A(12,17,18)	122.1968	D(4,5,6,11)	179.9907
R(25,26)	1.40	A(12,17,19)	113.5436	D(10,5,6,1)	-179.971
R(25,29)	1.07	A(18,17,19)	124.2595	D(10,5,6,11)	0.022
R(26,27)	1.39	A(17,18,22)	118.3421	D(4,9,12,13)	0.3206
R(26,31)	1.07	A(18,22,20)	107.5341	D(4,9,12,17)	-179.9208
R(27,28)	1.34	A(18,22,21)	113.1718	D(15,9,12,13)	-179.6454
R(27,32)	1.08	A(18,22,23)	111.6054	D(15,9,12,17)	0.1132
		A(20,22,21)	107.6883	D(17,18,22,20)	-110.7803
		A(20,22,23)	107.9547	D(17,18,22,21)	8.0251
		A(21,22,23)	108.6829	D(17,18,22,23)	131.0006
		A(25,24,30)	122.4911	D(18,22,23,24)	11.4782
		A(25,26,31)	121.2571	D(20,22,23,28)	72.5512
				D(21,22,23,28)	43.9832
				D(21,22,23,28)	-43.9832
				D(22,23,24,30)	-0.9395
				D(23,24,25,26)	-0.0583
				D(30,24,25,26)	179.9361
				D(24,25,26,27)	-0.0186
				D(30,24,25,26)	179.9361
				D(30,24,25,29)	-0.138
				D(25,26,27,28)	0.0791
				D(31,26,27,32)	0.0419
				D(26,27,28,23)	-0.0561

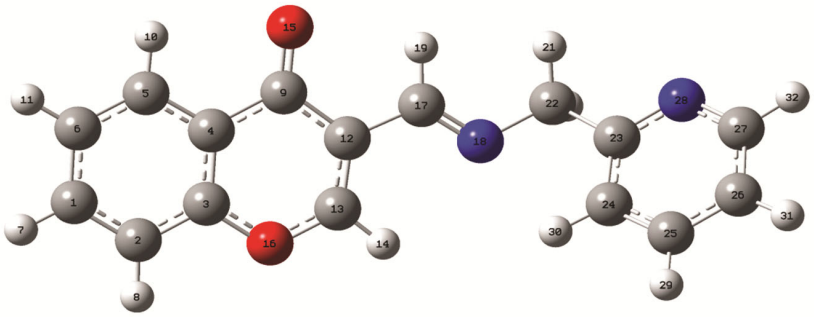

Fig. 1 — PMMC optimized structure with atom numbering

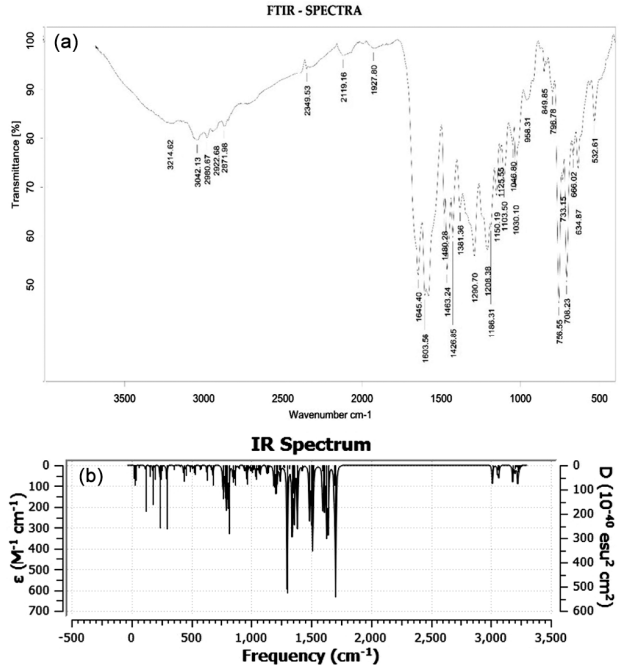

Fig. 2 (a-b) — Experimental IR spectrum of PMMC; Theoritical IR spectrum of PMMC

calculated molecular structure and atom numbering of PMMC from Table 1, we can notice that R (22, 23) is as long as 1.54Å which is close to a C-C bond. The bond length of R (17,18) is 1.07 Å indicating a double bond nature, but it is lesser than the normal C=N bond length. Furthermore, the R (9,15) bond length is 1.25 Å, indicating a double bond nature.

The calculated parameters of bond angles reveal that A (18,17,19) and A (12,13,16) are near to 124° indicating that the chromone ring is connected to the C17 atom. The dihedral angles of D (2,3,16,13), and D (4,5,6,11) are very close to 180°, showing the coplanar structure of the molecule with the chromone rings. D (4,3,16,13), D (3,4,5,6), D (10,5,6,11), D (4,9,12,13) and D (25,26,27,28) are almost at 0° or 180°, accordingly. The results demonstrate that the chromone ring and the pyridine ring are almost in the same plane, indicating this title molecule has a large conjugated system.

NMR spectral analysis

The following is a description of the NMR values derived from the observed spectra (Fig. 2). ^{1}H NMR ($CDCl_3$, 400 MHz): δ_H, 8.60 (1H, d, J = 7.6 Hz, Ar-H), 8.46 (2H, d, J = 8 Hz, Ar-H), 7.89-7.83 (1H, m, Ar-H), 7.80 (1H, d, J = 8.2 Hz, Ar-H), 7.62-7.59 (1H, m, Ar-H), 7.54-7.51 (2H, m, CH), 7.40-7.37 (2H, m, Ar-H), 2.39 (2H, s, -CH_2); The ^{1}H NMR signals in the range of 7.54–7.51 ppm are assigned to the imine proton and the coumarin proton. The signals between 8.60–7.37 ppm are attributed to the aromatic protons. The signal singlet at 2.39 ppm corresponds to the benzylic CH_2 protons. ^{13}C NMR ($CDCl_3$, 100 MHz): δ 177.1, 167.7, 158.2, 158.1, 155.5, 147.0, 144.6, 134.0, 132.1, 128.2, 127.5, 126.6, 125.4, 121.5, 55.5.

FT-IR spectra

The FT-IR analysis of PMMC is given in Fig. 3a. FT-IR spectra of PMMC exhibits peaks corresponding to C=O, C=N, and C-O linkages. This compound was experimentally showed a strong IR band at 1622 cm^{-1} (Ref. 28), which is corresponding to the azomethine, ν(HC=N) group. However, the calculated value of this band is found at 1666 cm^{-1}. The IR spectrum of the PMMC molecule showed the important absorption bands at the range of 1645-1640 cm^{-1}corresponds to (C=O), 1581-1443 cm^{-1} corresponding to (C=N), and 1406-1398 cm^{-1} corresponding to (C=C). Experimental values are in good agreement with theoretical values (Fig. 3b).

Mass spectra

In HRMS (Fig. 4), molecular ion peak obtained for the molecule was 265.09, corresponding to $[M+H]^+$ ion. This Spectral characterization and elemental

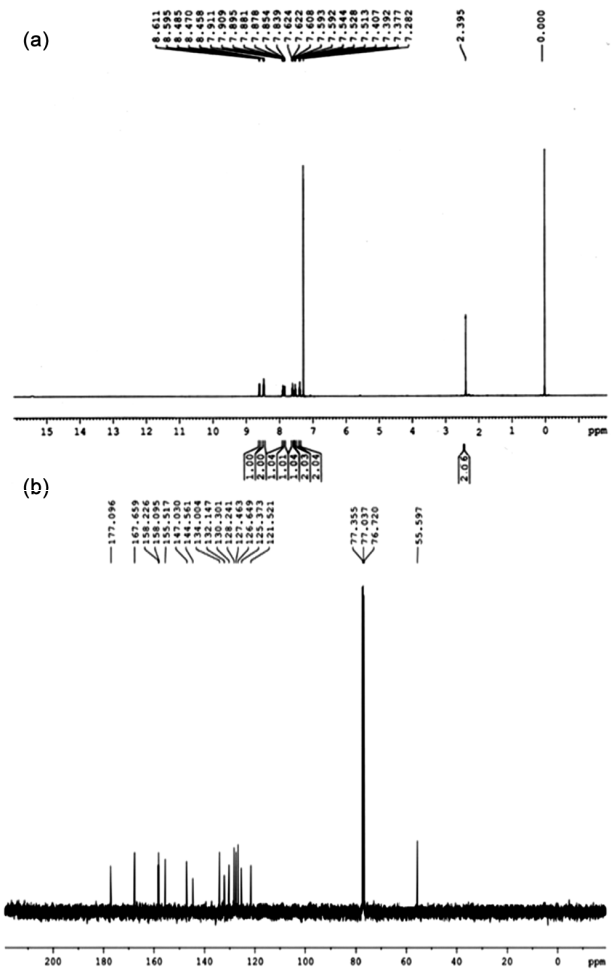

Fig. 3(a-b) — ^{1}H Experimental spectrum of PMMC; ^{13}C Experimental spectrum of PMMC

analysis confirms the structure and purity of this compound.

Natural bond orbital (NBO) analysis

NBO analysis was performed for PMMC at B3LYP/6-311++ G(d,p) functional level to elucidate the charge transfer, hyper conjugative interaction of Lewis orbital and non-Lewis orbital, the intramolecular hydrogen bonding and delocalization of π electron of the compound[29]. The second-order perturbation theory of the Fock matrix in the NBO analysis of the title molecule suggests the presence of the strong intra-molecular hyperconjugative interaction listed. For each acceptor (j) and donor (i), the stabilization energy E(2) associated with the delocalization from i → j is calculated as,

$$E(2) = -n_\sigma \frac{\langle \sigma \mid F \mid \sigma \rangle^2}{\varepsilon_\sigma * - \varepsilon_\sigma} = -n_\sigma \frac{Fij^{\,2}}{\Delta E} \qquad \ldots (1)$$

The population of the donor orbital is $\boldsymbol{\eta}_\sigma$ and the NBO orbitals fock matrix elements i and j are $<\sigma/F/\sigma>^2$, where σ and σ*are NBO orbitals and with energies are ε and ε*, From Table 2 there are several kinds of interactions exist in PMMC molecule. They are as follows, i) the interaction between lone pair of O16 (LP2) with anti-bonding σ* C12-C13, ii) lone pair of N18(LP1) with anti-bonding σ* C17-H19and iii) lone pair of O15 (LP1) with anti-bonding σ* C4-C9, and these interactions resulted the stabilization energies as 34.36kJ/mol., 10.57kJ/mol., and 19.65kJ/mol respectively. The greater electro negativity of oxygen and nitrogen atoms of chromone caused intra-molecular interactions. Clark *et al*., strongly recognized that the electron density around the substituted oxygen nucleus is more anisotropic and this causes oxygen atoms to participate in a variety of intermolecular interactions[30,31]. The interaction of $\boldsymbol{\pi}$*C3-C4 with $\boldsymbol{\pi}$*C1-C2 resulted in the high hyper-conjugation stabilization energy (276.81kJ/mol.). Table 2.

NLO Properties

The NLO active materials are approved much interest in current years with a view of their various optoelectronic applications. The wide range of applications of organic NLO materials rather than inorganic NLO materials is due to the suitable constructive properties for selective device application. These materials are simply susceptible to frequency change and large laser damage threshold and express optical sensing duration over inorganic NLO materials[32]. The relationship between a compound's structure and its nonlinear optical (NLO) activity can be evaluated through its total hyperpolarizability (βtotal) values. In the present study, the calculated β_{total} (Table 3) of PMMC (1224.5707×10^{-30}esu) is significantly larger than that of urea (0.1947×10^{-30} esu). From these results, it is revealed that the PMMC molecule exhibits strong NLO properties. This could be concluded from the earlier reports as a molecule that has higher β and lower HOMO-LUMO values possess enhanced NLO ativity[33].

Frontier molecular orbital analysis

Frontier molecular orbitals are also known as HOMO-LUMO, are vital in quantum chemistry and play an essential role in understanding properties like optical, electronic, reactivity, and chemical activity.

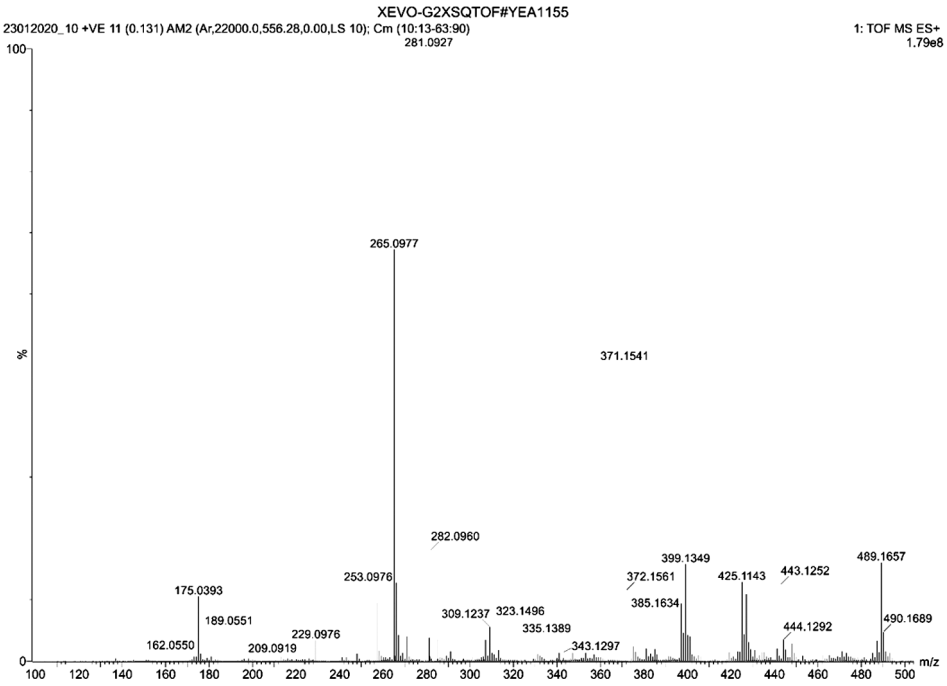

Fig. 4 — Mass spectrum of PMMC

Table 2 — The second order perturbation theory analysis of fock matrix in NBO basis of the title molecule with B3LYP/6-311 G++ (d, p)

Donor(i)	Type	ED i/e	Acceptor (j)	Type	ED i/e	E(2) (Kcal/mol)	E(i)-E (j)	E(Ij) (a.u.)
C1-C2	**σ**	1.97535	C1-C6	**σ** *	0.01670	2.69	1.27	0.052
			C1-H7	**σ** *	0.01063	1.24	1.19	0.034
			C2-C3	**σ** *	0.02270	3.05	1.28	.056
			C2-H8	**σ** *	0.01151	1.61	1.19	0.039
			C3-O16	**σ** *	0.03369	4.09	0.98	0.057
			C6-H11	**σ** *	0.01126	1.80	1.19	0.042
C1-C2	**π**	1.69055	C3-C4	**π***	0.30400	21.70	0.27	0.070
			C5-C6	**π***	0.27388	16.50	0.29	0.062
C1-C6	**σ**	1.98070	C1-C2	**σ** *	0.01529	2.81	1.28	0.054
			C1-H7	**σ** *	0.01063	1.22	1.17	0.034
			C2-H8	**σ** *	0.01151	2.24	1.17	0.046
			C5-C6	**σ** *	0.01528	2.88	1.29	0.055
			C5-H10	**σ** *	0.01632	2.22	1.19	0.046
			C6-H11	**σ** *	0.01126	1.18	1.18	0.033
C1-H7	**σ**	1.98365	C1-C2	**σ** *	0.01529	1.31	1.11	0.034
			C1-C6	**σ** *	0.01670	1.08	1.09	0.030
			C2-C3	**σ** *	0.02270	3.25	1.09	0.053
			C5-C6	**σ** *	0.27388	2.76	1.12	0.050
C2-C3	**σ**	1.967671	C1-C2	**σ** *	0.01529	2.72	1.31	0.053
			C1-H7	**σ** *	0.01063	1.88	1.21	0.043
			C2-H8	**σ** *	0.01151	1.47	1.20	0.038
			C3-C4	**σ** *	0.03424	5.36	1.29	0.074
			C4-C9	**σ** *	0.06770	2.59	1.19	0.050

(Contd.)

Table 2 — The second order perturbation theory analysis of fock matrix in NBO basis of the title molecule with B3LYP/6-311 G++ (d, p) (*Contd.*)

Donor(i)	Type	ED i/e	Acceptor (j)	Type	ED i/e	E(2) (Kcal/mol)	E(i)-E (j)	E(Ij) (a.u.)
			C13-016	σ *	0.03369	1.60	1.03	0.036
C2-H8	σ	1.97984	C1-C2	σ *	0.01529	1.62	1.11	0.038
			C1-C6	σ *	0.01670	2.83	1.09	0.050
			C2-C3	σ *	0.02270	1.26	1.09	0.033
			C3-C4	σ *	0.03424	3.48	1.09	0.055
			C3-O16	σ *	0.03369	1.14	0.79	0.027
C3-C4	σ	1.97465	C2-C3	σ *	0.01529	4.81	1.30	0.071
			C2-H8	σ *	0.01151	1.57	1.21	0.039
			C4-C5	σ *	0.02373	4.02	1.31	0.065
			C4-C9	σ *	0.06770	2.52	1.20	0.050
			C5-H10	σ *	0.01632	1.36	1.23	0.036
			C9-015	σ *	0.00775	1.64	1.25	0.041
C3-C4	π	1.63802	C1-C2	σ *	0.30400	17.02	0.29	0.064
			C3-C4	σ *	0.42870	1.25	0.28	0.017
			C5-C6	σ *	0.27388	17.97	0.30	0.067
			C9-O15	σ *	0.25392	20.14	0.28	0.069
C3-O16	σ	1.99103	C1-C2	σ *	0.01529	1.10	1.49	0.036
			C4-C5	σ *	0.02373	1.30	1.48	0.039
			C13-H14	σ *	0.01854	1.17	1.38	0.036
C4-C5	σ	1.96830	C3-C4	σ *	0.03424	4.60	1.26	0.068
			C3-O16	σ *	0.03369	4.05	0.96	0.056
			C4-C9	σ *	0.06770	2.82	1.16	0.052
			C5-C6	σ *	0.01528	2.77	1.29	0.054
			C5-H10	σ *	0.01632	1.10	1.19	0.032
			C6-H11	σ *	0.01126	2.03	1.18	0.044
			C9-C12	σ *	0.06424	1.00	1.17	0.031
C4-C9	σ	1.97618	C2-C3	σ *	0.01529	1.96	1.23	0.044
			C3-C4	σ *	0.03424	2.75	1.23	0.052
			C4-C5	σ *	0.02373	3.23	1.24	0.057
			C5-C6	σ *	0.01528	1.71	1.26	0.042
			C9-C12	σ *	0.06424	1.01	1.14	0.031
			C12-C17	σ *	0.03632	2.38	1.16	0.047
C5-C6	σ	1.98044	C1-C6	σ *	0.01670	2.73	1.27	0.053
			C1-H7	σ *	0.01063	1.90	1.18	0.042
			C4-C5	σ *	0.02373	3.28	1.28	0.058
			C4-C9	σ *	0.06770	2.58	1.17	0.050
			C5-H10	σ *	0.01632	1.58	1.20	0.039
			C6-H11	σ *	0.01126	1.41	1.19	0.037
C5-C6	π	1.67555	C1-C2	π *	0.30400	21.65	0.27	0.069
			C3-C4	π *	0.42870	19.26	0.26	0.065
C5-H10	σ	1.98072	C1-C6	σ *	0.01670	2.96	1.07	0.050
			C3-C4	σ *	0.03424	3.92	1.08	0.058
			C4-C5	σ *	0.02373	1.54	1.08	0.037
			C5-C6	σ *	0.01528	1.47	1.11	0.036
C6-H11	σ	1.98395	C1-C2	σ *	0.01529	2.88	1.10	0.050
			C1-C6	σ *	0.01670	1.10	1.08	0.031
			C4-C5	σ *	0.01670	3.15	1.09	0.052

(*Contd.*)

Table 2 — The second order perturbation theory analysis of fock matrix in NBO basis of the title molecule with B3LYP/6-311 G++ (d, p) (*Contd.*)

Donor(i)	Type	ED i/e	Acceptor (j)	Type	ED i/e	E(2) (Kcal/mol)	E(i)-E (j)	E(Ij) (a.u.)
			C5-C6	σ *	0.01528	1.46	1.11	0.036
C9-C12	σ	1.97643	C4-C5	σ *	0.02373	2.25	1.25	0.047
			C4-C9	σ *	0.06770	0.95	1.14	0.030
			C9-015	σ *	0.00775	0.57	1.19	0.023
			C12-C13	σ *	0.02586	3.39	1.30	0.059
			C12-C17	σ *	0.03632	1.74	1.16	0.040
			C13-H14	σ *	0.01854	2.07	1.15	0.044
			C17-N18	σ *	0.00704	1.49	1.28	0.039
C9-O15	σ	1.99555	C3-C4	σ *	0.03424	0.91	1.61	0.034
			C4-C9	σ *	0.06770	1.07	1.51	0.036
			C9-C12	σ *	0.06424	1.08	1.52	1.52
			C12-C13	σ *	0.02586	0.82	1.67	0.033
C9-O15	π	1.96586	C3-C4	π*	0.42870	5.92	0.35	0.046
			C12-C13	π*	0.21711	6.62	0.36	0.046
C12-C13	σ	1.98268	C9-C12	σ *	0.06424	3.33	1.25	0.058
			C9-015	σ *	0.00775	1.78	1.28	0.043
			C12-C17	σ *	0.03632	3.40	1.26	0.059
			C13-H14	σ *	0.01854	1.83	1.25	0.043
			C17-H19	σ *	0.04122	0.65	1.23	0.025
C12-C13	π	1.80483	C9-O15	π*	0.25392	22.16	0.30	0.073
			C12-C13	π*	0.21711	3.86	0.30	0.031
			C17-N18	π*	0.10040	14.98	0.31	0.063
C12-C17	σ	1.96925	C4-C9	σ *	0.06770	1.36	1.13	0.035
			C9-C12	σ *	0.06424	1.81	1.14	0.041
			C12-C13	σ *	0.02586	4.24	1.29	0.066
			C13-O16	σ *	0.03369	4.19	0.96	0.057
			C17-N18	σ *	0.00704	1.46	1.27	0.039
			N18-C22	σ *	0.01442	3.43	1.00	0.052
C13-H14	σ	1.98138	C3-O16	σ *	0.03369	2.96	0.82	0.04
			C9-C12	σ *	0.06424	4.76	1.03	0.063
			C12-C13	σ *	0.02586	2.86	1.18	0.052
C13-016	σ	1.99152	C2-C3	σ *	0.01529	1.81	1.48	0.046
			C12-C17	σ *	0.03632	1.89	1.41	0.046
C17-N18	σ	1.99241	C9-C12	σ *	0.06424	1.22	1.37	0.037
			C12-C17	σ *	0.03632	1.34	1.39	0.039
			C17-H19	σ *	0.04122	0.72	1.36	0.028
			N18-C22	σ *	0.01442	0.60	1.24	0.024
C17-N18	π	1.94672	C12-C13	π*	0.21711	9.02	0.32	0.050
C17-H19	σ	1.98813	C12-C13	σ *	0.02586	3.41	1.15	0.056
			C12-C17	σ *	0.03632	0.52	0.52	0.021
			C17-N18	σ *	0.00704	0.56	1.13	1.13
N18-C22	σ	1.98318	C12-C17	σ *	0.03632	4.26	4.26	0.063
			C17-N18	σ *	0.00704	0.52	1.29	0.023
			C23-N28	σ *	0.01891	2.02	2.02	0.044
H20-C22	σ	1.96219	C17-N18	σ *	0.00704	0.88	1.10	0.028
			C17-N18	π*	0.10040	3.18	0.52	0.037
			C22-C23	σ *	0.03592	0.67	0.90	0.022

(*Contd.*)

Table 2 — The second order perturbation theory analysis of fock matrix in NBO basis of the title molecule with B3LYP/6-311 G++ (d, p) (*Contd.*)

Donor(i)	Type	ED i/e	Acceptor (j)	Type	ED i/e	E(2) (Kcal/mol)	E(i)-E (j)	E(Ij) (a.u.)
			C23-C24	σ *	0.03592	0.82	1.08	0.027
			C23-N28	π*	0.38566	0.027	0.51	0.044
H21-C22	σ	1.98240	C22-C23	σ *	0.03592	0.69	0.90	0.022
			C23-C24	σ *	0.03592	2.05	1.08	0.042
			C23-N28	π*	0.38566	1.94	0.52	0.031
C22-C23	σ	1.97801	C17-N18	σ *	0.00704	0.93	1.22	0.030
			C17-N18	π*	0.10040	1.03	0.65	0.024
			H20-C22	σ *	0.01579	0.95	1.07	0.029
			H21-C22	σ *	0.02388	0.70	1.06	0.024
			C23-C24	σ *	0.03592	2.19	1.20	0.046
			C23-N28	σ *	0.01891	0.53	1.13	0.022
			C24-C25	σ *	0.01729	1.98	1.21	0.044
			C27-N28	σ *	0.01261	2.48	1.13	0.047
C23-C24	σ	1.98142	C22-C23	σ *	0.03592	1.98	1.11	0.042
			C23-N28	σ *	0.01891	1.27	1.21	0.035
			C24-C25	σ *	0.01729	2.98	1.30	0.056
			C24-H30	σ *	0.01901	1.52	1.21	0.038
			C25-H29	σ *	0.01174	2.17	1.19	0.045
C23-N28	σ	1.98616	N18-C22	σ *	0.01442	1.08	1.15	0.032
			C23-C24	σ *	0.03592	1.67	1.41	0.043
			C24-H30	σ *	1.98010	1.34	1.32	0.038
			C27-N28	σ *	0.01261	0.75	1.33	0.028
			C27-H32	σ *	1.98621	1.70	1.31	0.042
			H20-C22	σ *	1.96219	1.70	0.72	0.034
			H21-C22	σ *	1.98240	0.71	0.71	0.022
			C24-C25	π*	1.64738	14.81	0.31	0.060
			C26-C27	π*	1.65764	25.71	0.30	0.079
C23-N28	π	1.69710	C24-C25	π*	1.64738	14.81	14.81	0.060
			C26-C27	π*	1.65764	25.71	0.30	0.079
C24-C25	σ	1.97892	C22-C23	σ *	0.03592	2.97	1.10	0.051
			C23-C24	σ *	1.98142	3.16	1.28	0.057
			C24-H30	σ *	1.98010	1.49	1.19	0.038
			C25-C26	σ *	1.98039	2.87	1.28	0.054
			C25-H29	σ *	1.98505	1.22	1.18	0.034
			C26-H31	σ *	0.01323	2.17	1.18	0.045
C24-C25	π	1.64738	C23-N28	π*	1.69710	28.23	0.26	0.077
			C26-C27	π*	1.69710	18.54	0.27	0.064
C24-H30	σ	1.98010	C23-C24	σ *	1.97801	1.71	1.09	0.039
			C23-N28	σ *	1.98307	4.50	1.01	0.060
			C24-C25	σ *	0.01729	1.48	1.10	0.036
			C25-26	σ *	1.98039	2.65	1.09	0.048
C25-C26	σ	1.98039	C24-C25	σ *	0.01729	2.91	1.29	0.055
			C24-H30	σ *	1.98010	2.17	1.19	0.045
			C25-H29	σ *	1.98505	1.22	1.18	0.034
			C26-C27	σ *	1.98668	2.59	1.28	0.051
			C26-H31	σ *	1.98307	1.32	1.18	0.035
			C27-H32	σ *	1.98621	2.02	1.19	0.044

(*Contd.*)

Table 2 — The second order perturbation theory analysis of fock matrix in NBO basis of the title molecule with B3LYP/6-311 G++ (d, p) (*Contd.*)

Donor(i)	Type	ED i/e	Acceptor (j)	Type	ED i/e	E(2) (Kcal/mol)	E(i)-E (j)	E(Ij) (a.u.)
C25-H29	**σ**	1.98505	C23-C24	**σ** *	1.98142	2.82	1.10	0.050
			C24-C25	**σ** *	0.01729	1.26	1.11	0.033
			C25-C26	**σ** *	1.98039	1.18	1.10	0.032
			C26-C27	**σ** *	1.98668	2.67	1.10	0.049
C26-C27	**σ**	1.98668	C25-C26	**σ** *	1.98039	2.90	1.29	0.055
			C25-H29	**σ** *	1.98505	2.31	1.19	0.047
			C26-H31	**σ** *	1.98505	1.37	1.19	0.036
			C27-N28	**σ** *	1.98720	0.71	1.21	0.026
			C27-H32	**σ** *	1.98621	1.36	1.20	0.036
C26-C27	**π**	1.65764	C23-N28	**π***	1.98616	16.60	0.26	0.060
			C24-C25	**π***	1.64738	21.34	0.28	0.070
C26-H31	**σ**	1.98307	C24-C25	**σ** *	1.97892	2.64	1.11	0.048
			C25-C26	**σ** *	1.98039	1.31	1.10	0.034
			C26-C27	**σ** *	1.98668	1.21	1.10	0.033
			C27-N28	**σ** *	1.98720	3.79	1.02	0.056
C27-N28	**σ**	1.98720	C22-C23	**σ** *	1.97801	2.67	1.22	0.051
			C23-N28	**σ** *	1.98616	0.90	1.32	0.031
			C26-C27	**σ** *	1.98668	1.08	1.39	0.035
			C26-H31	**σ** *	1.98307	1.58	1.30	0.040
C27-H32	**σ**	1.98621	C23-N28	**σ** *	1.98307	3.43	1.02	0.053
			C25-C26	**σ** *	1.98039	3.08	1.10	0.052
			C26-C27	**σ** *	1.98668	1.02	1.10	0.030
LP(1)O15		1.97716	C4-C9	**σ** *	0.06770	19.65	0.68	0.10
			C9-C12	**σ** *	0.06424	18.99	0.70	0.10
LP(2)O16		1.70160	C3-C4	**σ** *	0.03424	28.44	0.34	0.09
			C12-C13	**σ** *	0.02586	34.36	0.34	0.09
LP(1)N18		1.90978	C12-C17	**σ** *	0.03632	4.08	0.81	0.05
LP(1)N18			C17-H19	**σ** *	0.04122	10.57	0.79	0.08
LP(1)N18			H21-C22	**σ** *	0.02388	5.04	0.77	0.05
C3-C4	**π***	0.42870	C1-C2	**π***	0.30400	276.81	0.01	0.08
C3-C4	**π***	0.42870	C5-C6	**π***	0.27388	142.27	0.02	0.08
C12-C13	**π***	0.21711	C17-N18	**π***	0.10040	79.61	0.01	0.06
C23-N28	**π***	1.98616	C24-C25	**π***	0.31047	176.09	0.02	0.08
C23-N28	**π***	1.98616	C26-C27	**π***	0.32020	214.67	0.01	0.07

ED/e is the electron density of donor and acceptor of NBO orbitals.
[a]E(2) means energy of hyper conjugative interaction (stabilization energy)
[b]*E(i) - E(j)* Energy difference between donor and acceptor i and j NBO orbitals.
[c]*F(i,j)* is the Fock matrix element between i and j
NBO orbitals. *i*: donor orbital, *j*: acceptor orbital, a.u : atomic unit, e; occupancy.

HOMO-LUMO energies and its band gap energy (ΔE) of the target molecule were investigated by using DFT calculations at B3LYP/6–311++G(d,p) level of theory in a gaseous state. The evaluated energies of HOMO, LUMO, and the band gap energy are found to be -6.335950 eV, -1.9564996 eV, and 4.6770954 eV as shown in Fig. 5. The small E_{HOMO}-E_{LUMO} band gap indicates that the molecule is soft, and has more chemical activity and low stability. Koopman's theorem states that the LUMO value is directly related to the electron affinity (A) and the HOMO energy is directly related to the ionization potential (I)[34]. The global molecular reactivity descriptors like chemical hardness (η), chemical softness (S), chemical potential (μ), and global electrophilicity index (ω) were evaluated from HOMO-LUMO orbital energies from the following equations[35] and are recorded in Table 4.

Table 3 — The values of calculated dipole moment (μ) polarizability (α) and first order hyperpolarisability (*β*)) PMMC molecule with B3LYP/6-311 G++ (d, p)

Parametre	6-311G++(d,p)
μx	0.8635616
μy	–1.3353461
μz	1.3353461
μt	2.078548
αxx	282.6563501
αxy	13.4256878
αyy	166.5008378
αxz	–7.1250189
αyz	5.6428067
αzz	73.1263258
Δα	1.608639×10^{-24}
βxxx	315.9359584
βxxy	259.4873872
βxyy	–1.3531299
βyyy	–65.1502184
βxxz	71.4937626
βxyz	–99.6102155
βyyz	24.2637444
βxzz	7.732285
βyzz	–0.6383872
βzzz	–25.4538925
βt	1224.5707×10^{-30}

However, *a* and *b* values of the Gaussian output are in atomic units (a.u.), so they have been converted into electronic units (e.s.u.), (*a*; 1 a.u. ¼ 0.1482×10^{-24} e.s.u., *b*; 1 a.u. ¼ 8.6393×10^{-33} e.s.u.)

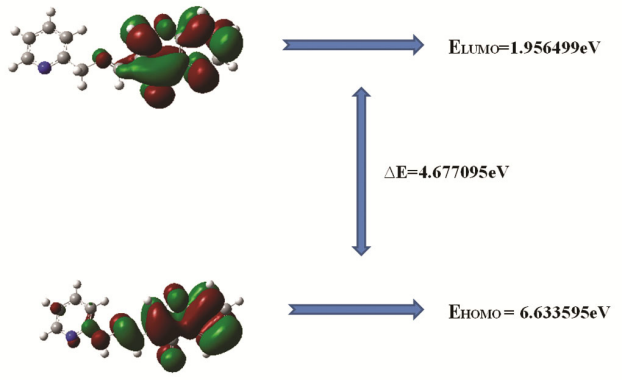

Fig. 5 — Representation of the optimized structures, HOMO, and LUMO of PMMC

The energy gap is used to calculate the following properties.

$A = -E_{LUMO}$

$I = -E_{HOMO}$

χ = (I+A) /2, (Electronegativity)

μ= - (I+A)/2, (Chemical potential)

η= (I-A)/2, (Chemical hardness)

Table 4 — Frontier molecular orbital energy values and chemical reactivity descriptor values of PMMC by B3LYP/6–311++G(d,p) method

Parameter	Formula	Chromone (in eV)
HOMO Energy (E1)	–	−6.335950 eV
LUMO Energy (E2)	–	−1.956499 eV,
EnergygapEg ($E_{HOMO}E_{LUMO}$)	E_2-E_1	4.677095 eV
Ionization energy (I)	$–E_1$	−6.335950 eV
Electron affinity (A)	$–E_2$	−1.956499 eV,
Global hardness (η)	Eg/2	2.338547eV,
Chemical softness (S)	$(E_1+E_2)/2$	–4.146224eV
Chemical potential (μ)	1/2η	1.169273eV
Electrophilicity index (ω)	$\mu^2/2\eta$	1.5986299eV

S= 1/2η, (Chemical softness)

ω= μ^2 /2 η (Electrophilicity index)

The frontier orbital band gap energy and chemical hardness (η) values show that intramolecular charge transfer is inhibited; if they are large, there is little to no charge exchange[36]. The calculated large value of chemical hardness and high value of band gap energy for PMMC exhibits that there is promising charge transfer in the molecule and proves that the molecule is biologically active. The electrophilicity index (ω) represents the measure of the energy reduction caused by the maximum charge transfer between the acceptor and donor.

Molecular electrostatic potential map (MESP) analysis

MESP elucidates the charge density of the compounds in three dimensions. To explore the molecular interactions in any compound, MESP plays a considerable role and it gives the negative and positive regions in the molecule that are nucleophilic and electrophilic attacking centers of the molecule[37,38]. At a point r, the MEP V(r) is represented as

$$V(r) = \Sigma N A |(Z A /|r - R A |) - \int \rho(ŕ)d 3 ŕ /|r - ŕ |- \quad ... (2)$$

Here N represents the total number of nuclei in the molecule. The MEP of PMMC was calculated and the results are shown in Fig. 6. The MESP of molecules changes with different colors *i.e.*, red, blue, green, and yellow, where the red color shows the maximum negative regions of electrostatic potential, and blue represents positive electrostatic potential[39,40]. Furthermore, in PMMC, the region around the nitrogen atom of the pyridine ring. In addition, oxygen atoms have more electronegative potential and the region around the hydrogen atom of a pyridine ring has positive electrostatic potential. Furthermore, the negative potential region is

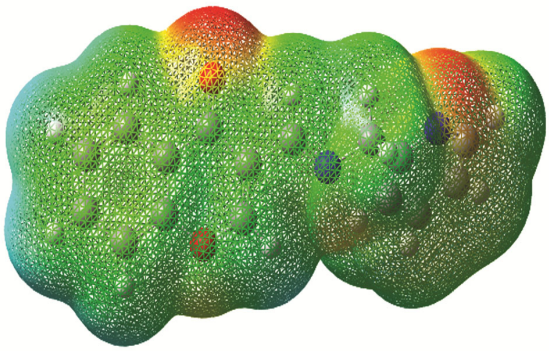

Fig. 6 — MESP map of PMMC

Table 5 — Mulliken Charges of PMMC by B3LYP/6–311++G(d,p) method.

S. No.	Atoms	Mulliken charges
1	C	–0.178045
2	C	–0.183858
3	C	0.291852
4	C	–0.054477
5	C	–0.168022
6	C	–0.183143
7	H	0.204623
8	H	0.215832
9	C	0.420658
10	H	0.225158
11	H	0.200776
12	C	–0.168136
13	C	0.144645
14	H	0.265516
15	O	–0.497629
16	O	–0.562854
17	C	0.147685
18	N	–0.492321
19	H	0.213654
20	H	0.213654
21	H	0.208473
22	C	–0.266661
23	C	0.271515
24	C	–0.203496
25	C	–0.147080
26	C	–0.237705
27	C	0.065618
28	N	–0.573533
29	H	0.197466
30	H	0.204385
31	H	0.189885
32	H	0.206065

electrophilic and the positive region potential region is nucleophilic for the molecules under exploration.

Mulliken charges

Mulliken charges are the entire charge tensor and the total charge flux tensor, which is known as the charge flux model[41]. The atomic charges moderately come out on the surface which could be introducing the whole chemical properties of the molecule[42]. The atomic charges on the various atomic sites of the title molecule have been computed using the DFT/B3LYP/6-311 ++ G(d,p) level. Table 5 represents the higher electro-negativity in differentiation with the other atoms. Here, the C3, C9, C13, C17, and C23 atoms accept the positive charge with magnitude 0.291 a.u.,0.420 a.u., 0.144 a.u.,0.147 and 0.271a.u. The remaining 11 carbon atoms of PMMC possess negative charge respectively. The two atoms of nitrogen N18 and N28, possess negative charges as -0.492 a.u., and -0.573 a.u. for the molecule. According to natural charge analysis, every hydrogen atom has the highest positive charge because of the strong electronegativity of the N atoms in the molecule. Furthermore, O15 and O16 oxygen atoms have a negative charge of -0. 497a.u and -0.562 a.u respectively.

ADMET predictions

Computational methods were useful in analyzing the different physicochemical features of pharmacokinetic descriptors, which were analyzed for PMMC compound through the online tool Molinspiration Cheminformatics server[44]. Drug similarity is the standard abstraction used for a drug-like property, these molecular properties are mainly hydrophobicity, electronic distribution, hydrogen bonding properties, and the existence of several pharmacological aspects that affect the molecular behavior of organisms, incorporate bioavailability, transport properties, interaction with proteins, reactivity, toxicity, metabolic stability, and many others[45]. Lipinski's rule of five was used to estimate the bioavailability of bulk materials to calculate the drug properties; this rule plays a major role in drug discovery. In the present work, the physiochemical properties study of bulk molecules was implemented with the Molinspiration Cheminformatics program. The drug-likeness of synthesized PMMC molecule was analyzed and presented in Table 6. The good membrane permeability of molecules should obey the following: H-bond donors (HBD) were found to be 0 (≤5), H-bond acceptors (HBA) were found to be 4(≤10), molecular weight is 264.28g/mol (≤500 g/mol), Vander Walls topological polar surface area (TPSA) value is 55.47 Å².So, the compound obeys Lipinski's rule of five for all cases. The bioactivity score of the compound was also calculated. From

Table 6 — Physicochemical and pharmacokinetics properties by ADMET parameters of PMMC

Properties	Value	Properties		Value
Mol. Weight	264.28g/mol	Absorption	HIA	97.913096
C log P	4.10		Caco2	28.0595
Log D*p*H7.4	5.4		MDCK	42.4326
Log S*p*H7.4	4.29	Distribution	GIabsorption	HIGH
Wsol	2.06 mg/m		BBB	1.2333
HBD	0	Metabolism	GPCR	-0.39
HBA	4		Ion CM	-0.38
TPSA	55.47 Å²		Kinase	-0.23
Nrot	2		Nuclear	-0.62
Csp3	0.06		Protease	-0.79
Nvio	0		Enzyme	0.18
Molar Refractivity	78.22	Toxicity	TA100-10RL$_I$	positive
			TA100-NA	Negative
			TA1535-10RL$_I$	Negative
			TA1535-NA	Negative
		CYP-2C19 inhibition		Inhibitor
		CYP-2C9 inhibition		Inhibitor
		CYP-2D6 inhibition		Non
		CYP-2D6 Substrate		Non
		CYP-3A4 inhibition		Non
		CYP-3A4 Substrate		Substrate
		Log KP(Skin permeation)		-3.43339

Table 6 and Fig. 7, the different properties were deciphered in ADMET analysis, including blood-brain barrier (BBB) penetration, human intestinal absorption (HIA), Caco-2 cell permeability, water solubility in the buffer, pure water solubility, skin permeability, MDCK cell permeability, P-glycoprotein inhibition, plasma protein binding, CYP (2C19, 2C9) inhibition, CYP (3A4) substrate, Ames test for mutagenicity, carcinogenicity (mouse, rat), human ether-a-go-go-related gene (hERG) inhibition, Lipinski' rule, WDI like rule, lead like rule, CMC like rule, and MDDR like rule[51]. SwissADME software was used to calculate the bioactive score and physical parameters correlated to the previously used drugs for cancer treatment. It has reduced potential to penetrate the BBB in the central nervous system, according to the penetration potential result. The obtained value is 1.2333 which indicates that the molecule causes some side effects in the central nervous system. HIA is one of the significant parameters for a drug molecule[46]. An HIA value between 90 and 100% shows good human intestinal absorption for this molecule, and it is 90.45%. Drug absorption through oral is predicted by two parameters: Caco-2 and MDCK cell permeability. The calculated Caco-2 cell permeability value is 28.0595nm/s and the MDCK cell permeability value

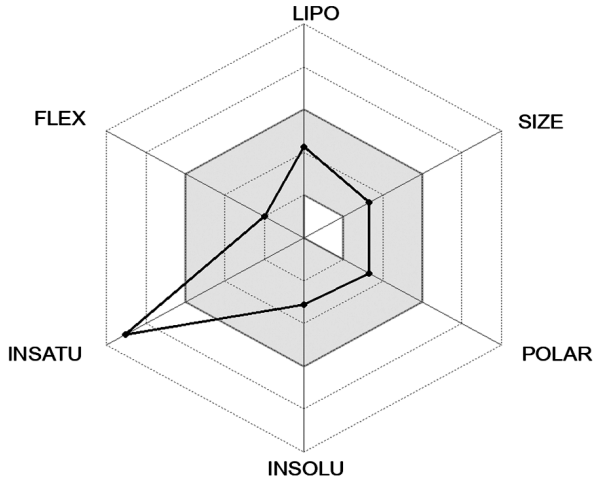

Fig. 7 — Bioavailability radar of PMMC by the druglikeness criteria (Lipophilicity (-0.7<log P<5.0), size (150 g/mol<MW < 500 g/mol), polarity (20 Å^2< TPSA < 130 Å^2), insolubility (-6<log S<0), insaturacao (0.25<Fraction Csp^3<1) and flexibility (0<Num. Rotatable bonds < 9)

is 42.4326 nm/s respectively. The inhibited P-glycoprotein value for the molecule shows that the inhibitor and the protein were responsible for the pharmacokinetic properties of the drug. The pure water solubility analysis was 2.06 mg/m. The cytochrome protein indicates that the molecule is an inhibitor of 2C19, and 2C9, which reduces the rug's

capability and pharmacological effects. It is found that the molecule is not an inhibitor of 2D6. The mutagenicity data by the Ames test for the molecule is positive for the isomers. Ames TA 100-10RL_I is positive. Moreover, TA 1535-10RL_I TA 100-NA, and TA 1535-NA is negative. The synthesized molecule does not cause cancer in mice but it is carcinogenic in rats. The molecule adheres to Lipinski's rule of five and according to the World Drug Index (WDI), the probability of its permeability and solubility is greater than 90%. The molecule also meets the lead-like rule, with a binding affinity greater than 0.1 μM. The qualifying range for the number of atoms in the molecule should be between 20 and 40. Since the molecule contains less than 40 atoms, it qualifies for the CMC-like rule.

Anti-fungal Activity

The synthesized PMMC compound was scrutinized for its *in vitro* anti-fungal activity against the fungal strains *Candida albicans, Fusarium oxysporum, Aspergillus flavus, and Aspergillus niger*. Compared with the standard drug Fluconazole with minimum inhibitory concentration (MIC) values. The results of *in vitro* anti-fungal activity in MIC of the tested compound showed outstanding anti-fungal activity against *Fusarium oxysporum, Aspergillus flavus, and Aspergillus niger* with values of 25 μg/mL, 25μg/mL, and 25μg/mL (Fig. 8, Table 7). The standard pathogenic microbial cultures were procured from the Microbial Type Culture Collection (MTCC), Chandigarh, India. The minimum inhibitory concentration (MIC) values for the tested compound, and standards were measured in μg/mL.

Anti-bacterial activity

Using the broth dilution method, *in vitro* antibacterial activity was demonstrated against two gram-positive bacteria, *Staphylococcus aureus* and *Bacillus subtilis*, and two gram-negative bacteria, *Klebsiella pneumoniae* and *Escherichia coli.* The Microbial Type Culture Collection (MTCC) in Chandigarh, India, is where the standard pathogenic microbial cultures were purchased. Both the standards and the tested drugs' minimum inhibitory concentrations (MIC) were expressed in μg/mL. It has been reported that PMMC has higher antibacterial activity. These results (Fig. 9) showed that PMMC showed moderate activity against the strains has a greater effect against *Escherichia coli* than the other bacteria. Four tested strains *Staphylococcus aureus* (25 μg/mL), *Bacillus subtilis* (25 μg/mL), *Klebsiella pneumoniae* (50 μg/mL) and *Escherichia coli* (>100 μg/mL) subtilis for the standard drug streptomycin. The title molecule shows good activity against the same organism under identical experimental conditions.

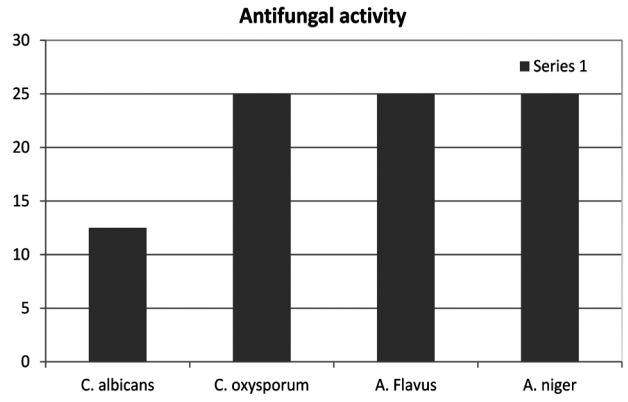

Fig. 8 — Antifungal activity of PMMC

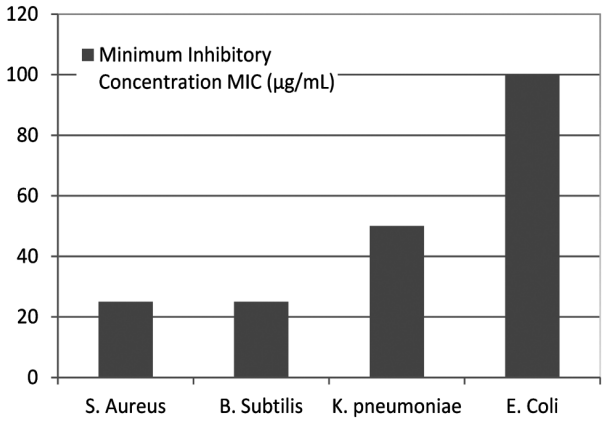

Fig. 9 — Antibacterial activity of PMMC

Table 7 — Anti microbial activity (MIC) of synthesized PMMC compound

Fungal sample	Minimum Inhibitory Concentration MIC (μg/mL)	Bacterial sample	Minimum Inhibitory Concentration MIC (μg/mL)
Candida albicans	12.5	*Staphylococcus aureus*	25
Fusarium oxysporum	25	*Bacillus subtilis*	25
Aspergillus flavus	25	*Klebsiella pneumoniae*	50
Aspergillus niger	25	*Escherichia coli*	>100

Table 8 — Antioxidant properties of test compounds against DPPH

Compd	IC50 (μg/mL)
PMMC	11.48 ± 1.86
Ascorbic acid	0.42 ± 1.07

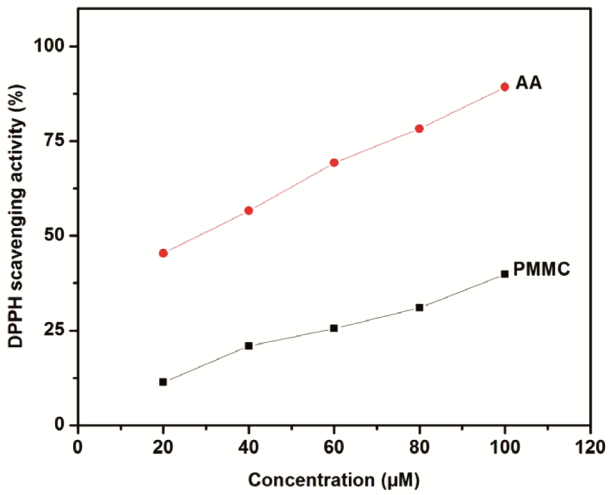

Fig. 10 — Radical scavenging activity of PMMC in comparison with standard ascorbic acid

Radical scavenging activity

In order to determine the DPPH free radical scavenging capacity of PMMC compound, 0.1 mM solution of DPPH in ethanol was prepared, and then 0.5 mL of this solution was added to 1.5 mL of the solution of the complexes in ethanol at different concentrations (ranging from 20 to 100 M). After that, these solutions were given a thorough whirl and allowed to incubate for half an hour in the dark. The absorbance of the produced solutions was measured at 517 nm after a further 30 minutes of waiting. The values for the compound PMMC that were computed to have a half minimum inhibitory concentration (IC_{50}) which was shown in Table 8 and Fig. 10. From the figure, it is clear that compound PMMC displayed a significant radical scavenging effect, on DPPH techniques with lower IC_{50} value. However, PMMC have lesser activity (11.48 ± 1.86 μg/mL) compared to the Ascorbic acid (0.42 ± 1.07 **μg/mL**). The information in Table 8 supports this. The ability of a chemical to transfer a hydrogen atom (HAT) is one of the factors that determine its DPPH scavenging action[47].

Conclusion

The structural and electronic properties of the PMMC derivative were successfully analyzed using the DFT/ B3LYP/6–311++G(d,p) level of theory. The optimized structural parameters, IR spectrum, and simulated NMR spectrum were calculated following the GIAO approach in DMSO-d6 solvent at the same level of DFT. The molecular orbital co-efficient analysis suggests that the electronic transitions are assigned to π-π* transitions. NBO analysis shows the stability and charge delocalization from various bonding to anti-bonding orbitals of the title molecule. Based on these findings, we conclude that the title compound may be a potential applicant in the development of NLO products. The reactive sites of the PMMC compound were identified from MESP and Mulliken atomic charges and E_{HOMO}-E_{LUMO} energies were determined. Drug likeness and ADMET properties were calculated for the title compound. The title molecule shows good activity against the antibacterial and antifungal organisms under identical experimental conditions. Additionally, the compound PMMC displayed a significant radical scavenging effect, in the DPPH assay with a lower IC_{50} value.

References

1 Schiff H & Liebigs J, *Ann Chem*, 131 (1864) 118.
2 Sreeja P B & Kurup M R P, *Spectrochim Acta A*, 61 (2005) 331. doi: 10.1016/j.saa.2004.04.001
3 Anitha C, Sumathi S, Tharmaraj P & Sheela C D, *International Journal of Inorganic Chemistry*, 493942 (2011) 8. https://doi.org/10.1155/ 2011/493942.
4 Sreeja P B. & Kurup M.R.P, *Spectrochim Acta A*, 61 (2005) 331.
5 Singh R. & Kaushik N K, *Spectrochim Acta A*, 65 (2006) 950.
6 Sahu R & Shah K, Mini Rev Med Chem, 24 (2024) 1632.
7 Lv L , Zheng T, Tang L, Wang Z, Liu W, *Cord Chem Rev*, 525 (2024) 216327,
8 Rehman S, Ikram M, Baker R J, Zubair M, Azad E, Min S, Riaz K, Mok K & Rehman S U, *Chem Cent J*, 15 (2013) 68.
9 Rawat A & Reddy A V B, *Eur J Med Chem Rep*, 5 (2022)100038.
10 Loncar M, Gaso-Sokac D & Molnar M, *Czech J Food Sci*, 41 (2023) 79.
11 Sahoo C R, Sahoo J, Mahapatra M, Lenka D, Sahu P K, Dehury B, Padhy R N, Kumar P S, *Arabian J Chem*, 14, (2021) 102922.
12 Kecel-Gunduz S, Budama-Kilinc Y, Bicak B, Gok B, Belmen B, Feray A, Cigdem Y, *Arabian J Chem*, 16 (2023) 104440.
13 Egan D, James P, Cooke D & O'Kennedy R, *Can Lett*, 118 (1997) 201.
14 Manolov I, Maichle-Moessmer C, Nicolova I & Danchev N, *Arch Pharm*, 339 (2006) 319.
15 Hu X L, Gao C, Xu Z, Liu M L, Feng L S & Zhang G D, *Curr Top Med Chem*, 18 (2018)114.
16 Gilani A H, Shaheen F, Saeed S A, Bibi S, Irfanullah, Sadiq M & Faizi S, *Phytomedicine*, 7 (2000) 423.

17 Pattanayak P, Rout S S, Res Chem, 7 (2024) 101327.
18 Lu P H, Liao T H, Chen Y H, Hsu Y L, Kuo C Y, Chan C C, Wang L K, Chern C Y & Tsai F M, *Molecules*, 23 (2022) 4054.
19 Magiatis P, Melliou E, Skatsounis A, Mitaku S, Renard P, Pierre A & A Atassi, *J Nat Prod*, 61 (1998) 982.
20 Schonberg A & Latif N, *J Am Chem Soc*, 76 (1954) 6208.
21 Jimenez M, Mateo J J & Mateo R, *J Chromat A*, 870 (2000)473.
22 Agarwal R, *Biochem Pharmacol*, 6 (2000) 1042.
23 Musicki B, Periers A M, Laurin P, Ferroud D, Benedetti Y & Lachaud S, *Bioor Med Chem Lett*, 10 (2000) 1695.
24 Sreerama R, Nukala S K, Nagavelli V R, Kavitha Natte & Narsimha Sirassu, *Russian J Bioorg Chem*, 49 (2023) 580.
25 Natte Kavitha & Alivelu Munagala, *Comp Theor Chem*, 1201 (2021) 113287.
26 Hehre W J, Radom L, Schleyer P R & Pople J A, *Initio Molecular Orbital Theory*, (Wiley, New York) 1986.
27 Wolinski K, Hilton K J F & Pulay P, *J Am Chem Soc*, 112 (1990) 8251.
28 Natte Kavitha, Munagala A & Tangeda S, *Chem Phy Impact Chem Phys Imp*, 8 (2024) 100602.
29 Elsayed S A, El-Hendawy A M, Mostafa S I, Jean-Claude B J, Todorova M & Butler I S, *Bioinorg Chem Appl*, 2010 (2010) 149149.
30 Arivazhagan M & Meenakshi R, *Spectrochim Acta A*, 91 (2012) 419.
31 Varsanyi G & Szoke S, *Vibrational Spectra of Benzene Derivatives*, (Academic Press, New York), 1969.
32 Weinhold F, *Encyclopedia of Computational Chemistry*, (John Wiley & Sons, Chichester, UK), 1998, p. 1792-1811.
33 Percy S J, Leela P, Hemamalini R, Muthu S & Al-Saadi A A, *Spectrochim Acta A*, 146 (2015) 177.
34 Mary Y S, Panicker C Y, Anto P L, Sapnakumari M, Narayana B & Sarojini B K, *Spectrochim Acta A Mol Biomol Spectro*, 135 (2015) 81.
35 Koopmans T A, *Physica*, 1 (1933) 104.
36 Ramesh G & Reddy B V, *J Mol Struc*, 1160 (2018) 271.
37 Sert Y, Gumus M, Gokce H, Kani I & Koca I, *J Mol Struc*, 1171 (2018) 850.
38 Reactivity, Structure, Scattering, & Energetics of Organic, Inorganic & Biological Systems (Plenum Press, New York), 1981.
39 Scrocco E, & Tomasi J, *J Adv Quan Chem*, 11 (1998) 115.
40 Politzer P & Daiker K. C, *Models for Chemical Reactivity in the Force Concept in Chemistry*, (Van Nostrand Reinhold, New York), 1981.
41 Kavitha N & Alivelu M, *Int J Sci Res Sci Tech*, 8 (2021) 668.
42 Ferreira M M C & Suto E, *J Phy Chem*, 96 (1992) 8844.
43 Dewar M J S, *The Molecular Orbital Theory of Organic Chem*istry, (McGraw- Hill & Inc, New York), 1969.
44 Lipinski C. A, Lombardo F, Dominy B. W & Feene P J, *Adv Drug Del Rev*, 23 (1997) 3.
45 Proudfoot J R, *Bioorg Med Chem Lett*, 12 (2002) 1647.
46 Singh H P, Mishra S S, Sharma C S & Kumar N, *Int J Pharm Tech Biotech*, 4 (2017) 10.
47 Mishra S. S, Kumar N, Sirvi G, Sharma C. S, Singh H. P & Pandiya H, *Pharm Chem J*, 4 (2017) 143.
48 Baliyan S, Mukherjee R, Priyadarshini A, Vibhuti A, Gupta A, Pandey R P & Chang C M, *Molecules*, 27(2022)1326.